Structural Basis for the Function of the β-Barrel Assembly-Enhancing Protease BepA

Mohammad Shahrizal [1,†], Yasushi Daimon [2,†], Yoshiki Tanaka [1,†], Yugo Hayashi [1], Shintaro Nakayama [1], Shigehiro Iwaki [1], Shin-ichiro Narita [3], Hironari Kamikubo [1], Yoshinori Akiyama [2] and Tomoya Tsukazaki [1]

*1 - **Nara Institute of Science and Technology,** Ikoma, Nara 630-0192, Japan*
*2 - **Institute for Frontier Life and Medical Sciences,** Kyoto University, Kyoto 606-8507, Japan*
*3 - **Faculty of Nutritional Sciences,** University of Morioka, Iwate 020-0694, Japan*

***Correspondence to Yoshinori Akiyama and Tomoya Tsukazaki:** yakiyama@infront.kyoto-u.ac.jp, ttsukazaki@mac.com*
https://doi.org/10.1016/j.jmb.2018.11.024
Edited by Georg Schulz

Abstract

The β-barrel assembly machinery (BAM) complex mediates the assembly of β-barrel membrane proteins in the outer membrane. BepA, formerly known as YfgC, interacts with the BAM complex and functions as a protease/chaperone for the enhancement of the assembly and/or degradation of β-barrel membrane proteins. To elucidate the molecular mechanism underlying the dual functions of BepA, its full-length three-dimensional structure is needed. Here, we report the crystal structure of full-length BepA at 2.6-Å resolution. BepA possesses an N-terminal protease domain and a C-terminal tetratricopeptide repeat domain, which interact with each other. Domain cross-linking by structure-guided introduction of disulfide bonds did not affect the activities of BepA *in vivo*, suggesting that the function of this protein does not involve domain rearrangement. The full-length BepA structure is compatible with the previously proposed docking model of BAM complex and tetratricopeptide repeat domain of BepA.

Introduction

Gram-negative bacteria, including *Escherichia coli*, possess two layers of biological membranes, namely, the outer membrane and the inner membrane, between which exists the periplasmic space containing a peptidoglycan layer [1]. The two membranes act as a barrier to protect cells from changes in the external environment and hazardous substances. In addition, these membranes are involved in several stress responses, including the activation of the σ^E factor, which occurs on the cytoplasmic side, by monitoring the changes in the states of the outer membrane and the periplasm [2–5]. The outer membrane, which possesses an asymmetric architecture, is mainly composed of phospholipids on the inner leaflet and lipopolysaccharides on the outer leaflet, together with peripherally associated lipoproteins and embedded β-barrel proteins. All β-barrel outer-membrane proteins are synthesized in the cytoplasm, translocated across the inner membrane *via* the Sec complex, and inserted into the outer membrane *via* the β-barrel assembly machinery (BAM) complex [6–8], where they are converted into folded mature forms.

Precursors of outer-membrane proteins with an N-terminal signal peptide that are targeted to the inner membrane are initially synthesized by ribosomes and transferred to the Sec machinery, which consists of SecA ATPase, SecYEG complex, and SecDF [9,10]. Following their transfer, the machinery drives the translocation of unfolded precursor proteins across the inner membrane using the ATP hydrolysis energy and proton motive force. The signal sequence is cleaved by the signal peptidase during this process, and the processed proteins are released into the periplasm. At the final stage, the proteins are inserted into the outer membrane *via* the BAM complex and assembled while undergoing quality control and the assistance of targeting to the membrane by periplasmic chaperones/proteases such as Skp, DegP, SurA, and

FkpA, resulting in their conversion into functional β-barrel proteins [11–13]. The central, essential component of the BAM complex is an evolutionarily conserved β-barrel protein BamA [14], which belongs to the Omp85 protein family, which includes Sam50 in mitochondria and Toc75 in chloroplast. *In E. coli*, BamA forms a complex with four lipoproteins, namely, BamB, BamC, BamD, and BamE [6–8].

The σ^E-dependent stress response, which is an essential regulation system in *E. coli,* is activated by the accumulation of misfolded outer-membrane proteins. One of 114 genes identified as members of *E. coli* σ^E regulon encodes a periplasmic protein BepA (formerly YfgC) [5]. A BepA-deficient *E. coli* strain was shown to be more sensitive to specific antibiotics than wild-type cells, presumably due to the disrupted barrier functions of the outer membrane. Studies of the biogenesis of a β-barrel outer-membrane protein LptD, which is involved in the transport and assembly of lipopolysaccharides, suggest that BepA is related to the biogenesis and quality control of LptD [15,16]. LptD, which has two intramolecular disulfide bonds in its mature form, undergoes disulfide bond rearrangement during its biogenesis. BepA promotes this rearrangement and degrades incorrectly folded LptD. Impairment in biosynthesis of BepA-dependent LptD would cause reduction of the outer membrane barrier functions, leading to increased drug sensitivity of the cells. In addition, it was proposed that BepA interacts with the BAM complex to act in LptD folding and degrades a stalled LptD on the BAM complex. BepA was also proposed to cleave BamA that is misassembled during its biogenesis under a chaperone (SurA)-depleted condition [15–17]. These results suggest that BepA functions as a chaperone for outer-membrane protein biogenesis and as a protease for the removal of misfolded outer-membrane proteins.

The mature $BepA_{28–487}$ (MW ~51,000) protein, which is generated by cleavage of the signal peptide from the precursor form, is composed of an N-terminal protease domain and a tetratricopeptide repeat (TPR) domain. According to the MEROPS protein database [18], the protease domain is classified under the metalloprotease M48C subfamily, which shares a HEXXH motif. The active center is proposed to be formed by a Zn atom and residues H136, E137, and H140 of the HEXXH motif and E201 of the following C-terminal side (Fig. S1). Mutations H136R or E137Q in the HEXXH motif affect LptD biogenesis, implying that protease activity is crucial for BepA function [15]. Deletion mutants of the TPR domain abolish the activities of BepA, indicating that the TPR domain is also essential [16]. The crystal structure of the TPR domain revealed that 10 successive anti-parallel alpha-helices formed a large palm structure with a negatively charged pocket and a small palm structure with a cavity [16]. Generally, TPR domains provide a pocket for interactions with partners [19,20]. However, the interactions between the pocket of the BepA TPR domain and a substrate have not been elucidated to date. In contrast, site-specific photocrosslinking experiments revealed that several points at the edges of the TPR domain interact with Bam proteins and LptD. Based on these results, a model of the BAM complex with the TPR domain of BepA was proposed (Fig. S2) [16]. However, in order to unravel the underlying molecular mechanism in detail, the full-length structure of BepA is needed. In this study, we determined the full-length structure of BepA and proposed a functional mechanism for its activity in consideration of the stability of this protein in solution.

Results and Discussion

Overall structure of full-length BepA

Initial phases were calculated by molecular replacement with the crystal structures of the BepA TPR domain (PDB ID 5XI8) [16] and a Zn-dependent peptidase Q74D82 (PDB ID 3C37) from *Geobacter sulfurreducens*. The crystal structure of $BepA_{45–482}$ at 2.6-Å resolution was modeled with R_{work} = 21.5% and R_{free} = 25.9% (Fig. 1, Table 1). The asymmetric unit of the *P*1 space group contains six BepA molecules (designated Mol A–F), the superimpositions of which showed that the overall structures exhibit no significant structural change, with an RMSD of 0.47–0.82 Å for the Cα atoms (Fig. S3). Here, we discuss the structure of BepA using Mol B, which has the clearest electron density map among Mol A–F. The crystal structure of BepA consists of two domains: the N-terminal residues 45–288 form a M48C protease domain with 11 α-helices (α1–α11) and a β-sheet with three β-strands (β1–β3) between α2 and α3 (Figs. 1a, 1b, and S1), similar to the zinc peptidase Q74D82 (PDB ID 3C37); the successive C-terminal residues 305–482 form the TPR domain with 10 anti-parallel α-helices (H1–H10) in accordance with the previously reported TPR domain structure [16] (Fig. S4). The α12 tightly links the α11 of the protease domain and the H1 of the TPR domain. The residues 153–159 between α5 and α6 and residues 178–191 between α6 and α7 were not modeled because of the poor electron density (Fig. 1b, dotted line). The α-helices H1, H3, and H5 in the N-terminal region of the TPR domain are strongly associated with α-helices α2, α11, and α12 in the protease domain *via* hydrophobic/hydrophilic interactions, resulting in a 1126-$Å^2$ interaction area between the 45–304 and 305–390 residues. The C-terminal regions of the TPR domain show several interactions with the protease domain, including the formation of hydrogen bonds between the O of N68 and Nδ2 of N411, between Nη1 of R61 and the O of L439, and between Oε1 of Q51 and Nη1 of R480, creating a 505-$Å^2$ surface area between the 45–304 and 391–482 residues (Fig. 1b).

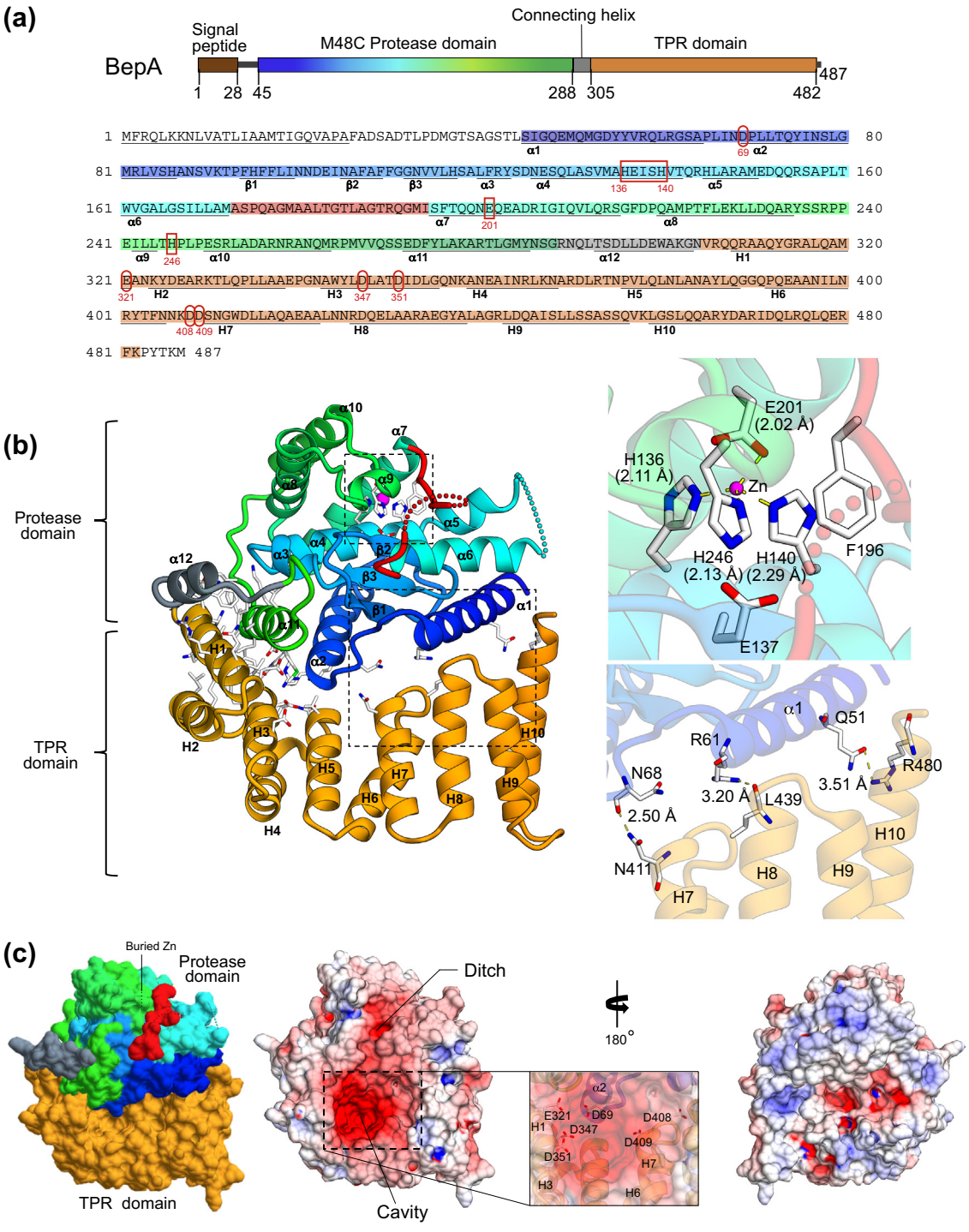

Fig. 1. Crystal structure of BepA. a, Schematic representation and amino acid sequence of BepA. α Helices (α1–12 and H1–10) and β strands (β1–3) are shown. The protease active site motif, HEXXH, and Zn-coordinated residues are highlighted by red boxes. Residues contributing to the negative cavity are labeled by red ellipses. b, Overall structure and close-up views. The protease domain is indicated in various colors, from blue to green. The connecting helix and TPR domains are colored in gray and orange, respectively. The side chains interacting with other domains are represented as a stick model. The zinc atom in the active center is coordinated by side chains of H136, H140, H246, and E201 (upper left). The C-terminal region of the TPR domain interacts with α1 of the protease domain *via* hydrogen bonds (lower right, dashed yellow line). c, Surface representation. The surfaces are colored as in panel B (left). The other surfaces are colored to indicate electrostatic potential ranging from blue (+10 *kT*/*e*) to red (−10 *kT*/*e*). The orientations are the same as panel b (left and middle). The acidic residues in the negatively charged cavity are represented as a stick model.

Table 1. Data collection and refinement

	BepA
Wavelength (Å)	1.00
Resolution range	48.18–2.598 (2.691–2.598)
Space group	*P*1
Unit cell	
a, *b*, *c* (Å)	85.844, 104.674, 104.971
α, *β*, *γ* (°)	113.606, 105.843, 104.026
Total reflections	327,914 (31,495)
Unique reflections	89,522 (8738)
Multiplicity	3.7 (3.6)
Completeness (%)	98.24 (94.90)
Mean *I*/sigma (*I*)	8.88 (0.86)
Wilson *B*-factor	62.50
R-merge	0.1039 (1.218)
R-meas	0.1219 (1.434)
R-pim	0.06328 (0.7477)
$CC_{1/2}$	0.997 (0.402)
CC*	0.999 (0.757)
Reflections used in refinement	89,487 (8729)
Reflections used for *R*-free	2016 (195)
R-work	0.2064 (0.3456)
R-free	0.2634 (0.3687)
CC (work)	0.964 (0.646)
CC (free)	0.944 (0.511)
Number of non-hydrogen atoms	19,732
Macromolecules	19,568
Ligands	54
Solvent	110
Protein residues	2485
RMS (bonds)	0.004
RMS (angles)	0.62
Ramachandran favored (%)	97.87
Ramachandran allowed (%)	2.09
Ramachandran outliers (%)	0.04
Rotamer outliers (%)	0.15
Clashscore	9.18
Average *B*-factor	81.27
Ligands	86.44
Solvent	56.41
Number of TLS groups	35

Statistics for the highest-resolution shell are shown in parentheses.

Active site of BepA

In the present crystal structure of BepA, the active site motif of the protease domain, H^{136}EISH, has one zinc atom that is coordinated by two histidine residues (H136 and H140) of the α4 helix, one glutamate residue (E201) residue of the α7 helix, and one histidine residue (H246) of the α9–α10 loop (Fig. 1b). The sequence alignment of full-length BepA with a Zn-dependent peptidase Q74D82 (PDB ID 3C37) indicates that the sequence identity is about 28% (Fig. S1), while the superimposition of BepA and Zn-dependent peptidase Q74D82 structures shows 1.77 Å of RMSD for the Cα atoms (Fig. S4). Therefore, the overall architectures of the protease domain of BepA and Q74D82 are similar. The residues coordinating the zinc atom of the active site in Q74D82, whose positioning is also essentially similar to that of BepA, are two histidine residues of H^{106}EINH, E162, and H208 (Figs. S4 and S1). The molecular mechanisms of proteolysis by BepA and Q74D82 are expected to be similar. Although the loop between the α6 and α7 helices of BepA is partially disordered (Fig. 1b, red), the C-terminal region of the loop seems to cover the active site. In the crystal structure of BepA, the activity of this protein would be low as the Zn atom of the active site is buried and the surrounding residues sterically interfere with the interaction between the active site and substrates. It is proposed that when BepA exhibits protease activity, the loop is dislocated in response to interactions with substrates or an unidentified factor, which enables unfolded regions of substrates to approach the protease active site. The dynamics of the loop covering the active site may adequately regulate the protease activity.

TPR domain and central cavity of BepA

Although the overall architecture of the TPR domain in the full-length structure of BepA is similar to that of the previously reported isolated TPR domain [16], reflecting an RMSD (1.67 Å) of the superimposition in Fig. S4, the TPR domain in the full-length structure is slightly extended compared with that of the isolated TPR domain, presumably due to the interaction with the protease domain (Fig. S4B). In the full-length structure, the negatively charged cavity of the TPR domain faces the protease domain (Fig. 1c), resulting in a characteristic cavity that is larger than that of the isolated TPR structure [16]. The hydrophilic cavity, which is about 20.2 Å × 12.5 Å wide and 14.6 Å deep at its maximum, includes D69 in α1–α2 loop of the protease domain, E321 in H1 helix, D347 and D351 in H3 helix, and D408 and D409 in H6–H7 loop (Fig. 1c). In addition, a negatively charged ditch protruding from the cavity leads to the area near the active site. Because TPR domains generally provide binding surfaces [19,20], the negativity charged regions of BepA may provide interaction sites for positively charged parts of substrates.

The crystal structure of BepA reflects its active form in solution

We performed small-angle X-ray scattering (SAXS) analysis of BepA to verify whether its conformation in an aqueous solution is the same as that of its crystal structure. The experimental scattering curve and the three-dimensional shape model of BepA based on SAXS data were adequately fitted with the BepA crystal structure (Figs. 2a and S5). However, we cannot exclude the possibility that BepA function involves alteration of the interaction between the protease and TPR domains; the dissociation of its domains may be necessary for its function. To confirm the conformation of BepA *in vivo*, we performed disulfide bond cross-linking analysis using BepA mutants. We selected five pairs of N-terminal amino and C-terminal residues that

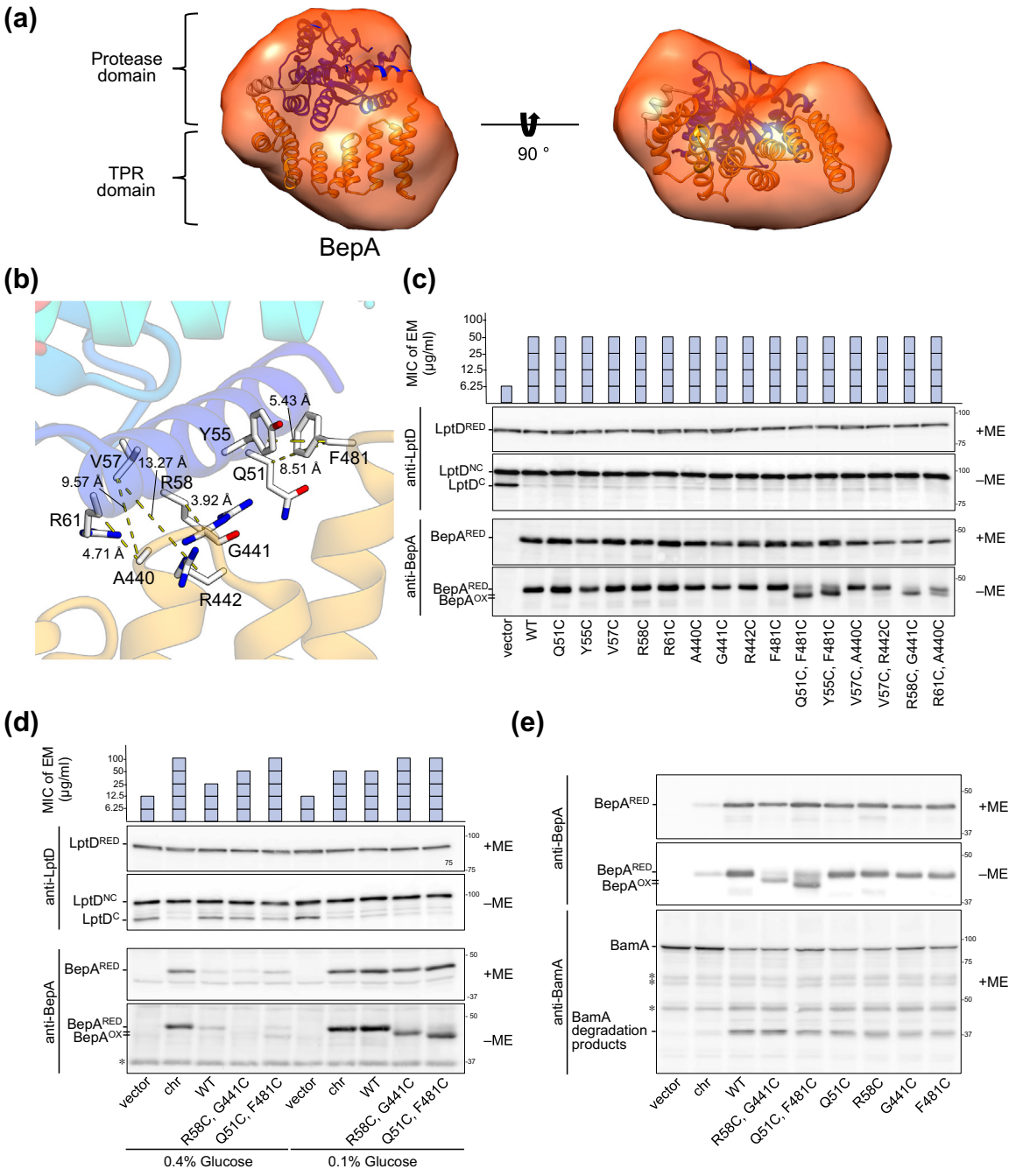

Fig. 2. Crystal structure of BepA reflects its active form in solution. (a) SAXS analysis of BepA in solution. The crystal structure was superimposed on the shape reconstruction of BepA based on SAXS data. (b) Close-up view of the N-terminal and C-terminal regions. The positions that were substituted by Cys were mapped on the crystal structure. (c and d) Intramolecular disulfide-bonded BepA mutants retain the chaperone-like activity of BepA. Accumulation of LptD and BepA (middle and bottom) and EM sensitivity (upper) of the Δ*bepA* cells expressing the individual BepA double cysteine mutants were determined. Wild-type cells carrying pUC18 (chr) or Δ*bepA* cells carrying pUC18 (vector), pUC-bepA (WT), or a derivative of pUC-bepA having the single or double cysteine mutations at the indicated positions in panel B were grown at 30 °C in L medium. The medium was supplemented with 0.1% or 0.4% glucose in panel d. Total cellular proteins were analyzed by SDS-PAGE under a reducing (+ME) or a non-reducing (–ME) condition and immunoblotting. The minimum inhibitory concentration of EM for each of the cells expressing BepA or its derivative was examined as described in Methods. (e) Degradation of BamA by double cysteine BepA mutants. The Δ*surA* cells carrying pUC18 (chr) or the Δ*surA* Δ*bepA* cells carrying pUC18 (vector), pUC-bepA (WT), or a derivative of pUC-bepA harboring the double cysteine mutation were grown at 30 °C in M9 medium supplemented with 1 mM IPTG. Total cellular proteins were analyzed as above. $LptD^{NC}$, $LptD^{C}$, and $LptD^{RED}$ indicate LptD with the non-consecutive disulfide bonds (the mature form), LptD with the consecutive disulfide bonds (a folding intermediate), and reduced LptD, respectively. $BepA^{RED}$ and $BepA^{OX}$ indicate reduced BepA and oxidized BepA, respectively. The asterisks indicate non-specific bands serving as a loading control.

are proximal within 13.3 Å (Fig. 2b) and introduced single and double cysteines into the indicated positions in Fig. 2b. The formation of intramolecular disulfide bonds between the cysteine residues restricts the flexibility of the N-terminal and C-terminal domains: BepA mutants possessing disulfide bonds can stably exist *in vivo* with a conformation similar to the crystal structure. First, we detected the accumulation and migration of BepA mutants over-expressed in the Δ*bepA* strain (Fig. 2c). The double-cysteine mutants Q51C–F481C, Y55C–F481C, R58C–G441C, and R61C–A440C show highly migrated bands ($BepA^{OX}$) on non-reducing SDS-PAGE. These bands disappeared under reducing conditions and the single-cysteine mutants did not exhibit such highly migrated bands, indicating that the double-cysteine mutants formed intramolecular disulfide bonds *in vivo*. The higher mobility of the BepA mutants possessing an intramolecular disulfide bond would be ascribed to the more compact conformations of these proteins than that of wild-type BepA. In addition, any upshifted bands due to disulfide bond formation were not observed (Fig. S6), suggesting that no intermolecular crosslink product between the BepA mutants was formed. In this experiment, it is reasonable that two pairs located more than 9 Å distant in the crystal structure did not form a disulfide bond. Furthermore, we examined the ability of the BepA mutants to enhance LptD maturation. Although the absence of BepA (vector) caused the accumulation of $LptD^{C}$, a folding intermediate, whose intramolecular disulfide bonds (C31–C173 and C724–C725) are different from those of mature $LptD^{NC}$ (C31–C724 and C173–C725) [15,16,21], all of the BepA mutants retained the LptD maturation-enhancing activity (Fig. 2c). Next, we examined the properties of erythromycin (EM) sensitivity of Δ*bepA* cells expressing the BepA mutants. The cells without BepA showed increased sensitivity to EM (Fig. 2c, vector), whereas all of the cells expressing BepA mutants exhibited EM resistance, similar to that of wild-type BepA (Fig. 2c). Although most of the Q51C–F481C and R58C–G441C mutant BepA molecules spontaneously formed an intramolecular disulfide bond, some amount of the mutant proteins remains reduced. Therefore, it cannot be ruled out that these reduced molecules are responsible for the above observed activities. To make sure that the BepA with a disulfide bond indeed possesses the activities comparable to normal (reduced) BepA, we lowered the accumulation of BepA proteins by adjusting the glucose concentration of the medium to repress expression from the *lac* promoter and examined their activities (Fig. 2d). In the presence of 0.1% glucose, the levels of the plasmid-expressed BepA were as low as that of the chromosomally encoded BepA (chr), but the mutant proteins were able to decrease $LptD^{C}$ accumulation and increase EM resistance of the cells (Fig. 2d, 0.1% glucose). Under this condition, a small amount of the reduced form of the mutant BepA proteins still accumulated. However, their levels were significantly lower than that of WT BepA in the presence of 0.4% glucose (Fig. 2d, WT, 0.4% glucose *versus* mutants, 0.1% glucose) that were not sufficient to exhibit the normal BepA activities. This result suggested that the disulfide-bonded BepA mutants retain their chaperone-like activities. Finally, we confirmed the protease activity of BepA (Fig. 2e), showing that all BepA mutants generated the degradation products of BamA that is probably misassembled in Δ*surA* cells. In addition, a comparison of the R58C/G441D mutant with chromosome-encoded BepA (chr), which showed little BamA degradation, indicates that at least the disulfide-bonded R58C/G441C mutant is active in substrate degradation (Fig. 2e). Taken together, BepA mutants were found to retain the chaperone-like and protease activities regardless of the presence or absence of disulfide bonds between the N-terminal and C-terminal regions; that is, the crystal structure of BepA reflects its active form in solution. It is suggested that BepA can function without the dissociation between the independent protease and TPR domains *in vivo*, and the crystal structure represents both its functional and resting states.

Putative functional model of BepA

In this paper, the full-length structure of BepA was determined at 2.6-Å resolution by X-ray crystallography and modeled by SAXS in aqueous solution. Our functional analyses revealed that BepA showed activity *in vivo* without large conformational transitions involving the dissociation of the protease and TPR domains. Daimon *et al.* [16] previously proposed a three-dimensional model of BepA and the BAM complex based on cross-linking results and the crystal structure of the TPR domain (Fig. S1). Indeed, this previously described model lacks the protease domain. Here, we superimposed the structure of full-length BepA onto the previous model [16] based on positions of each TPR domain. The orientation of BepA was slightly modified to avoid clashes between the BAM complex and BepA (Fig. 3a). The positions of the TPR domains in the previous and new models are similar. Therefore, the interaction sites between the BAM complex and BepA, which were identified by photocrosslinking experiments, are reasonably positioned in the new model as well. The protease domain protrudes to the periplasm side from the outer membrane. Here, we discuss the molecular mechanism of BepA in combination with the BAM complex based on the new model. It has been proposed that substrate proteins interact with BamD, the POTRA domain of BamA, and BepA [16,22–24]. This model shows a space between them, which may temporarily capture a proportion of the unfolded substrates. The flexible POTRA domain [25] may undergo large structural changes during integration of the outer-membrane proteins into the outer membrane; accordingly, the site may be larger and

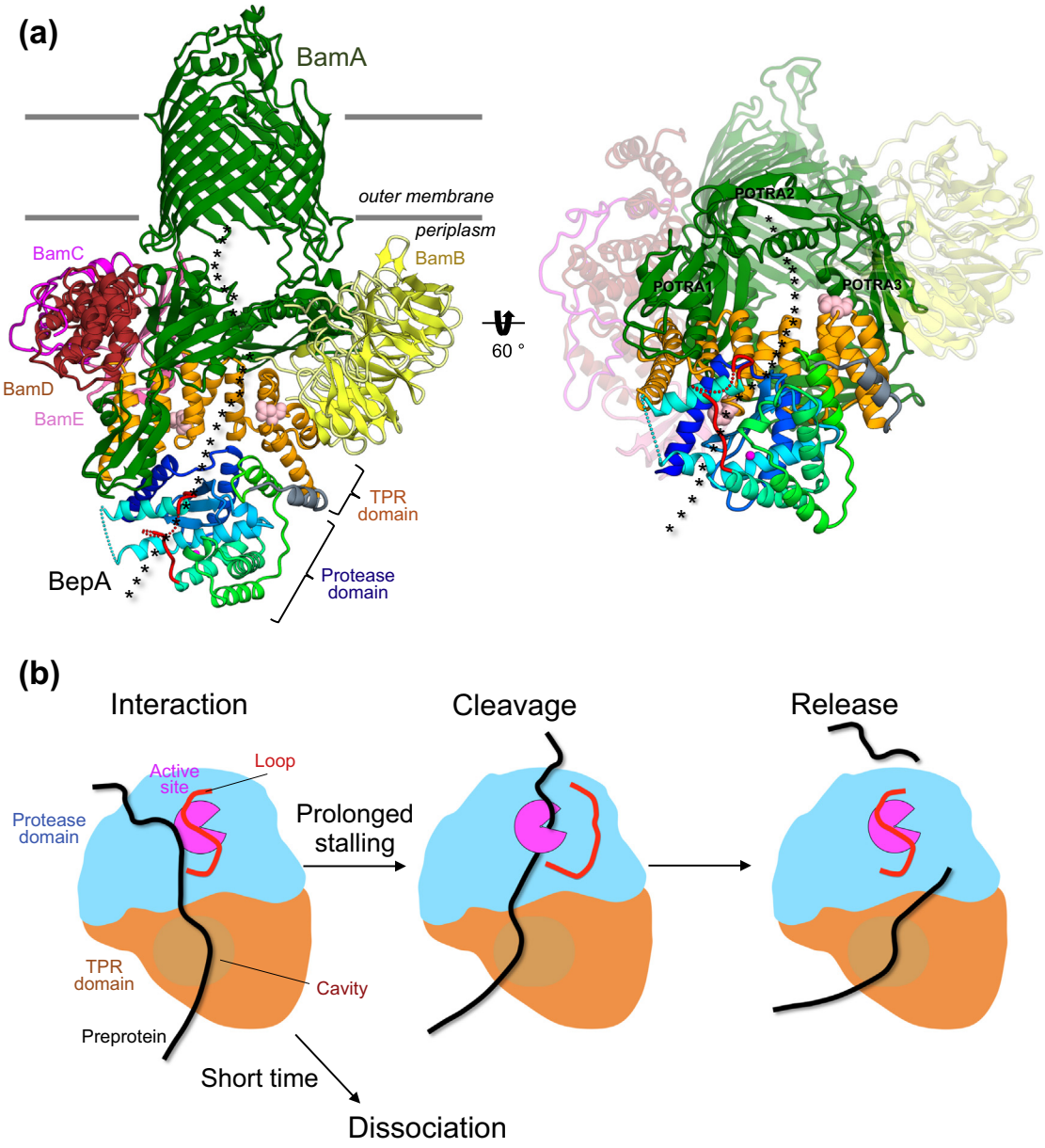

Fig. 3. Working model of BepA. (a) Docking model of the BAM complex and BepA. LptD-interaction sites were mapped onto the BepA structure [16]. The asterisks represent a putative substrate-interaction area described in the text. (b) Substrate-cleavage model of BepA. The TPR domain might provide the negatively charged interaction site for the substrate. The active site of the protease domain is covered by the flexible loop (red). When substrates interact with BepA for a prolonged duration, the frequency of the contact with the protease active site would increase with time, resulting in the eventual cleavage of the substrate by BepA, which contributes to the quality control of biogenesis for outer-membrane proteins.

interact with larger proteins than the space in the model. The negatively charged cavity of BepA (Fig. 1c) may interact with the positively charged parts of substrates; however, this remains to be confirmed. The previously reported interaction sites of BepA with LptD are located at the edge of the cavity [16], which is consistent with the idea that the substrate proteins interact with the cavity. The negatively charged cavity and protruded ditch (Fig. 1c) might interact with the histidine, arginine, and lysine residues of the substrate. The unfolded substrate protein may integrate into the membrane from the lateral gate of BamA in a stepwise fashion after interacting with BepA and the POTRA domain of BamA in the budding model, or the integration of the temporarily folded substrate protein into the membrane may be mediated by BepA and the BAM complex in the assisted model [11,12]. The chaperone activity of BepA may be important during these reactions. If the

transportation of a substrate stops midway, the substrate may be stalled for a long time in the area indicated by the asterisks shown in Fig. 3a. The short helices α5, α6, and α9, which includes H246, and loops near the active site of BepA may be flexible (Fig. 1a); it is conceivable that they are sometimes dislocated stochastically or in response to some unidentified signals. The prolonged stalling of the substrate at this position may result in a higher probability of its interaction with the active site resulting from the dislocation of the loops and short helices. Therefore, the long-stalled substrate protein at the same position may be cleaved by the protease domain of BepA. The loop structure on the active site of BepA may play an important role in prolonging the duration of transport of the substrate to the active site; this stalling may result in the substrate being cleaved (Fig. 3b). This notion is consistent with the idea that BepA digests stalled proteins [17]. To elucidate the molecular mechanism underlying BepA activity, it is necessary to perform detailed analysis of the interaction at the amino-acid residue level of BepA and the substrate protein, and to obtain structural information for the full complex of BepA and the BAM complex.

Methods

Expression and purification of BepA

The pYD296 plasmid, which was modified from pET-16b-TEV [16], encodes MG-H_{10}-SSGENLYFQG-*E. coli* $BepA_{45–482}$. *E. coli* strain KRX strain cells (Promega) were transformed with pYD296 and stored at −80 °C as a glycerol stock until use. The pre-cultured *E. coli* cells in 25 mL of LB Broth, Lennox (Nacalai) supplemented with 50 μg/mL ampicillin and 0.4% glucose at 37 °C for 12 h were inoculated into 2.5 L of LB broth, Lennox supplemented with ampicillin, and cultured at 37 °C until OD_{600} ~ 0.6. Then, protein expression was induced by 0.2% rhamnose. The culture was transferred into a 17 °C incubator and shaken for 12 h. The cells were harvested by centrifugation at 6000*g* for 10 min (Hitachi CR22N) and suspended in 10 mM Tris–HCl (pH 7.0). The washed cells were retrieved by centrifugation at 6000*g* for 10 min as a pellet and resuspended in sonication buffer [20 mM Tris–HCl (pH 7.0), 500 mM NaCl, 20 mM imidazole–HCl (pH 7.0), 1 mM 2-mercaptoethanol (ME), and 0.1 mM phenylmethanesulfonyl fluoride (PMSF)], together with 0.5 mM EDTA (pH 8.05). Cells were disrupted by sonication using Q500 (QSONICA) (20% power, pulse rate: 1 s on and 1 s off, rod: CL 334) for 30 min and centrifuged (20,400*g*, 30 min) at 4 °C. The supernatant was mixed with 3 mL of Ni Sepharose Excel (GE Healthcare) equilibrated with 20 mM Tris–HCl (pH 7.0), 500 mM NaCl, 20 mM imidazole–HCl (pH 7.0), 1 mM 2-ME, and 0.1 mM PMSF and rotated for 1 h at 4 °C. The resin was washed with 50 mL of wash buffer [20 mM Tris–HCl (pH 7.0), 500 mM NaCl, 20 mM imidazole–HCl (pH 7.0), 1 mM 2-ME, and 0.1 mM PMSF] and eluted with 40 mL of 20 mM Tris–HCl (pH 7.0), 500 mM NaCl, 300 mM imidazole–HCl (pH 7.0), 1 mM 2-ME, and 0.1 mM PMSF with different batches. TEV protease was mixed with the eluted proteins, with a protein weight ratio of 1:1 (1 mg of TEV protease to 1 mg of protein) and dialyzed against 20 mM Tris–HCl (pH 7.0), 500 mM NaCl, 1 mM 2-ME, and 0.1 mM PMSF at 4 °C for 12 h using a dialysis membrane [Spectra/Por 7 MWCO 10 kD (SPECTRUM)]. The cleaved protein was then incubated with 3 mL of Ni Sepharose Excel (GE Healthcare) by rotation before being washed from the polyhistidine-tag with 20 mM Tris–HCl (pH 7.0), 500 mM NaCl, 20 mM imidazole–HCl (pH 7.0), 1 mM 2-ME, and 0.1 mM PMSF. The cleaved protein was then concentrated using an Amicon Ultra 50 K filter (Millipore) and applied to a Superdex 200 Increase 10/300 column (GE Healthcare) equilibrated with 20 mM Tris–HCl (pH 7.0), 500 mM NaCl, 1 mM 2-ME, and 0.1 mM PMSF. For crystallization, the purified sample was concentrated to 17 mg/mL.

Crystallization of BepA

A volume of 0.1 μL of 17 mg/mL purified BepA was incubated at 4 °C by the sitting drop vapor diffusion method against a reservoir solution of 2 M ammonium sulfate in 96-well Violamo crystallization plates (plate model number: VCP-1). The crystallization plate was set up using Crystal Gryphon (Art Robbins Instruments). Microcrystals appeared after a 24-h incubation at 4 °C; then, the plate was incubated at 37 °C overnight to dissolve the microcrystals, followed by incubation at 4 °C for 2 days. Single rod-shaped crystals grew to a size of approximately 90 μm × 15 μm in 5 days. The crystals were collected using crystal harvesting mounts and loops (MiTeGen) and directly cryo-cooled in liquid nitrogen before performing X-ray diffraction experiments.

Data collection and determination of structure

The X-ray diffraction data set of the BepA crystal was collected by the Helical Data Collection Method on beamline BL32XU at SPring-8 using a microbeam [26]. The collected diffraction images were processed with XDS [27]. Initial phase was calculated by molecular replacement with the previously determined BepA TPR domain (PDB ID 5XI8) [16] and a Zn-dependent peptidase Q74D82 (PDB ID 3C37) as templates using Phaser [28]. We found independent six BepA molecule in the asymmetric unit by connecting the peptidase domain and the TPR domain based on the SAXS model. The structural model of BepA was stepwise-refined using COOT [29] and PHENIX [30]

to R_{work}/R_{free} = 0.206/0.263 with space group *P*1 at 2.6 Å resolution. A Ramachandran plot was constructed using Molprobity [31], and molecular graphics were generated using CueMol2 (http://www.cuemol.org/).

SAXS analysis

The SAXS measurements were carried out at the beamline BL-10C, Photon Factory (Tsukuba, Japan) [32]. Scattering images were collected from buffer (containing 20 mM Tris–HCl, 500 mM NaCl, 1 mM DTT, 0.1 mM PMSF, pH 7) and BepA solutions at 5 different concentrations (3.3, 6.5, 9.8, 12.7, and 15.9 mg/mL) at 20 °C. Ovalbumin (45 kDa; Sigma-Aldrich) was also measured to estimate the apparent molecular weight of BepA. The 60 scattering images were collected using a PILATUS3 2M detector (Dectris), where the exposure time for each image is 15 s. The 2D images were converted into 1D profiles using SAngler software [33]. The scattering profile averaging the first 10 frames among the 60 frames, where no radiation damage was observed at every concentration, was subject to the following analysis. The Guinier plots of BepA (Fig. S5A) did not show a steeper curve at the low Q-region, suggesting that no obvious aggregation occurred. The Rg^2 and the forward scattering intensity normalized by the weight per volume (mg/mL), I(0)/conc. were extrapolated to obtain values at zero protein concentration (Fig. S5B). The scattering profile at zero protein concentration was also calculated from extrapolation of the five scattering profiles at the different concentrations using the SVD implemented to Igor software (WaveMetrics). The scattering profiles at the higher Q-region (> 0.12 Å^{-1}) did not exhibit a clear dependence on concentration. The profile at the highest concentration at the high Q-region was merged into the profile at zero protein concentration. The maximum dimension was calculated using GNOM software [34]. The parameters from the above analyses were summarized in the Table S2. *Ab initio* shape modeling was performed using DAMMIF to obtain 20 models without structural restrictions such as point symmetry and particle anisometry [35]. Using the average model of the 20 models as a starting model, we finally refined the shape model using DAMMIN [36]. The refinement procedures were independently performed three times to confirm reproducibility. Figure 2a shows the representative model, into which the crystal structure of BepA is superposed using Situs software [37].

Functional analyses of BepA

The preparation of media was as described previously [16]. *E. coli* K12 strains and plasmids used in this study are listed in Supporting Information Table S2 [15,38,39]. Derivatives of pUC-bepA encoding a mutant form of BepA were constructed by site-directed mutagenesis. For determination of minimum inhibitory concentration of EM, overnight cultures were diluted 10^3-fold with L-medium, and 5 μL of these cultures was inoculated on L medium-based agar plates supplemented without or with 0.1% or 0.4% glucose and containing 6.25, 12.5, 25, 50, and 100 μg/mL EM. The plates were incubated for 18–20 h at 30 °C.

Accession number

Coordinates and structure factors have been deposited in the Protein Data Bank under accession number 6AIT.

CRediT authorship contribution statement

Mohammad Shahrizal: Methodology, Investigation, Writing - original draft. **Yasushi Daimon:** Conceptualization, Methodology, Investigation. **Yoshiki Tanaka:** Methodology, Investigation. **Yugo Hayashi:** Methodology, Investigation. **Shintaro Nakayama:** Methodology, Investigation. **Shigehiro Iwaki:** Methodology, Investigation. **Shin-ichiro Narita:** Conceptualization. **Hironari Kamikubo:** Methodology, Investigation. **Yoshinori Akiyama:** Conceptualization, Supervision, Writing - original draft. **Tomoya Tsukazaki:** Conceptualization, Supervision, Writing - original draft.

Acknowledgments

We thank K. Abe and S. Suzuki for secretarial assistance; K. Kobayashi and K. Yoshikaie for technical support; T. Lithgow, T. Shiota, and S. Matsuyama for antisera; and the beamline scientists at BL32XU of SPring-8 (Hyogo, Japan) for helping with data collection. The synchrotron radiation experiments were performed at BL32XU of SPring-8 with the approval of the Japan Synchrotron Radiation Research Institute (Proposal Nos. 2017A2557 and 2017B2557). The SAXS experiments were performed under the approval of the Photon Factory Program Advisory Committee (Proposal No. 2016G077). This work was supported by the JSPS/MEXT KAKENHI (Grant Nos. JP26119007, JP18H02405, JP17H05669, JP15H04350, JP18H02404, and JP18KK0197), Mitsubishi Foundation, Noguchi Institute, Naito Foundation, Mochida Memorial Foundation for Medical and Pharmaceutical Research, Joint Usage/Research Center program of Institute for Frontier Life and Medical Sciences Kyoto University.

Appendix A. Supplementary data

Supplementary data to this article can be found online at https://doi.org/10.1016/j.jmb.2018.11.024.

Received 31 August 2018;
Received in revised form 13 November 2018;
Accepted 26 November 2018
Available online 3 December 2018

Keywords:
outer membrane;
protein biogenesis;
protease;
chaperon;
crystal structure

†These authors contributed equally.

Abbreviations used:
BAM, β-barrel assembly machinery; TPR, tetratricopeptide repeat; SAXS, small-angle X-ray scattering; EM, erythromycin; PMSF, phenylmethanesulfonyl fluoride; ME, 2-mercaptoethanol.

References

[1] H. Nikaido, Molecular basis of bacterial outer membrane permeability revisited, Microbiol. Mol. Biol. Rev. 67 (2003) 593–656.
[2] G. Rowley, M. Spector, J. Kormanec, M. Roberts, Pushing the envelope: extracytoplasmic stress responses in bacterial pathogens, Nat. Rev. Microbiol. 4 (2006) 383–394.
[3] N.P. Walsh, B.M. Alba, B. Bose, C.A. Gross, R.T. Sauer, OMP peptide signals initiate the envelope-stress response by activating DegS protease via relief of inhibition mediated by its PDZ domain, Cell 113 (2003) 61–71.
[4] S. Lima, M.S. Guo, R. Chaba, C.A. Gross, R.T. Sauer, Dual molecular signals mediate the bacterial response to outer-membrane stress, Science 340 (2013) 837–841.
[5] S. Bury-Mone, Y. Nomane, N. Reymond, R. Barbet, E. Jacquet, S. Imbeaud, A. Jacq, P. Bouloc, Global analysis of extracytoplasmic stress signaling in *Escherichia coli*, PLoS Genet. 5 (2009), e1000651.
[6] M.G. Iadanza, A.J. Higgins, B. Schiffrin, A.N. Calabrese, D.J. Brockwell, A.E. Ashcroft, S.E. Radford, N.A. Ranson, Lateral opening in the intact beta-barrel assembly machinery captured by cryo-EM, Nat. Commun. 7 (2016) 12865.
[7] Y. Gu, H. Li, H. Dong, Y. Zeng, Z. Zhang, N.G. Paterson, P.J. Stansfeld, Z. Wang, Y. Zhang, W. Wang, C. Dong, Structural basis of outer membrane protein insertion by the BAM complex, Nature 531 (2016) 64–69.
[8] L. Han, J. Zheng, Y. Wang, X. Yang, Y. Liu, C. Sun, B. Cao, H. Zhou, D. Ni, J. Lou, Y. Zhao, Y. Huang, Structure of the BAM complex and its implications for biogenesis of outer-membrane proteins, Nat. Struct. Mol. Biol. 23 (2016) 192–196.
[9] A. Tsirigotaki, J. De Geyter, N. Sostaric, A. Economou, S. Karamanou, Protein export through the bacterial Sec pathway, Nat. Rev. Microbiol. 15 (2017) 21–36.
[10] T. Tsukazaki, Structure-based working model of SecDF, a proton-driven bacterial protein translocation factor, FEMS Microbiol. Lett. 365 (2018).
[11] A. Konovalova, D.E. Kahne, T.J. Silhavy, Outer Membrane Biogenesis, Annu. Rev. Microbiol. 71 (2017) 539–556.
[12] N. Noinaj, J.C. Gumbart, S.K. Buchanan, The beta-barrel assembly machinery in motion, Nat. Rev. Microbiol. 15 (2017) 197–204.
[13] J. De Geyter, A. Tsirigotaki, G. Orfanoudaki, V. Zorzini, A. Economou, S. Karamanou, Protein folding in the cell envelope of *Escherichia coli*, Nat. Microbiol. 1 (2016) 16107.
[14] N. Noinaj, A.J. Kuszak, J.C. Gumbart, P. Lukacik, H. Chang, N.C. Easley, T. Lithgow, S.K. Buchanan, Structural insight into the biogenesis of beta-barrel membrane proteins, Nature 501 (2013) 385–390.
[15] S. Narita, C. Masui, T. Suzuki, N. Dohmae, Y. Akiyama, Protease homolog BepA (YfgC) promotes assembly and degradation of beta-barrel membrane proteins in *Escherichia coli*, Proc. Natl. Acad. Sci. U. S. A. 110 (2013) E3612–E3621.
[16] Y. Daimon, C. Iwama-Masui, Y. Tanaka, T. Shiota, T. Suzuki, R. Miyazaki, H. Sakurada, T. Lithgow, N. Dohmae, H. Mori, T. Tsukazaki, S. Narita, Y. Akiyama, The TPR domain of BepA is required for productive interaction with substrate proteins and the beta-barrel assembly machinery complex, Mol. Microbiol. 106 (2017) 760–776.
[17] G.R. Soltes, N.R. Martin, E. Park, H.A. Sutterlin, T.J. Silhavy, Distinctive roles for periplasmic proteases in the maintenance of essential outer membrane protein assembly, J. Bacteriol. 199 (2017).
[18] N.D. Rawlings, A.J. Barrett, P.D. Thomas, X. Huang, A. Bateman, R.D. Finn, The MEROPS database of proteolytic enzymes, their substrates and inhibitors in 2017 and a comparison with peptidases in the PANTHER database, Nucleic Acids Res. 46 (2018) D624–D632.
[19] R.K. Allan, T. Ratajczak, Versatile TPR domains accommodate different modes of target protein recognition and function, Cell Stress Chaperones 16 (2011) 353–367.
[20] N. Zeytuni, R. Zarivach, Structural and functional discussion of the tetra-trico-peptide repeat, a protein interaction module, Structure 20 (2012) 397–405.
[21] S.S. Chng, M. Xue, R.A. Garner, H. Kadokura, D. Boyd, J. Beckwith, D. Kahne, Disulfide rearrangement triggered by translocon assembly controls lipopolysaccharide export, Science 337 (2012) 1665–1668.
[22] S. Kim, J.C. Malinverni, P. Sliz, T.J. Silhavy, S.C. Harrison, D. Kahne, Structure and function of an essential component of the outer membrane protein assembly machine, Science 317 (2007) 961–964.
[23] P.Z. Gatzeva-Topalova, T.A. Walton, M.C. Sousa, Crystal structure of YaeT: conformational flexibility and substrate recognition, Structure 16 (2008) 1873–1881.
[24] C.L. Hagan, J.S. Wzorek, D. Kahne, Inhibition of the beta-barrel assembly machine by a peptide that binds BamD, Proc. Natl. Acad. Sci. U. S. A. 112 (2015) 2011–2016.
[25] P.J. Fleming, D.S. Patel, E.L. Wu, Y. Qi, M.S. Yeom, M.C. Sousa, K.G. Fleming, W. Im, BamA POTRA domain interacts with a native lipid membrane surface, Biophys. J. 110 (2016) 2698–2709.
[26] K. Hirata, Y. Kawano, G. Ueno, K. Hashimoto, H. Murakami, K. Hasegawa, T. Hikima, T. Kumasaka, M. Yamamoto, Achievement of protein micro-crystallography at SPring-8 Beamline BL32XU, J. Phys. Conf. Ser. 425 (2013).
[27] W. Kabsch, Xds, Acta Crystallogr. D Biol. Crystallogr. 66 (2010) 125–132.
[28] A.J. McCoy, R.W. Grosse-Kunstleve, P.D. Adams, M.D. Winn, L.C. Storoni, R.J. Read, Phaser crystallographic software, J. Appl. Crystallogr. 40 (2007) 658–674.

[29] P. Emsley, K. Cowtan, Coot: model-building tools for molecular graphics, Acta Crystallogr. D Biol. Crystallogr. 60 (2004) 2126–2132.
[30] P.D. Adams, R.W. Grosse-Kunstleve, L.W. Hung, T.R. Ioerger, A.J. McCoy, N.W. Moriarty, R.J. Read, J.C. Sacchettini, N.K. Sauter, T.C. Terwilliger, PHENIX: building new software for automated crystallographic structure determination, Acta Crystallogr. D Biol. Crystallogr. 58 (2002) 1948–1954.
[31] V.B. Chen, W.B. Arendall III, J.J. Headd, D.A. Keedy, R.M. Immormino, G.J. Kapral, L.W. Murray, J.S. Richardson, D.C. Richardson, MolProbity: all-atom structure validation for macromolecular crystallography, Acta Crystallogr. D Biol. Crystallogr. 66 (2010) 12–21.
[32] N. Igarashi, Y. Watanabe, Y. Shinohara, Y. Inoko, G. Matsuba, H. Okuda, T. Mori, K. Ito, Upgrade of the small angle X-ray scattering beamlines at the Photon Factory, J. Phys. Conf. Ser. 272 (2011), 012026.
[33] N. Shimizu, K. Yatabe, Y. Nagatani, S. Saijo, T. Kosuge, N. Igarashi, Software development for analysis of small-angle X-ray scattering data, AIP Conference Proceedings, 1741, 2016 , (050017).
[34] D.I. Svergun, Determination of the regularization parameter in indirect-transform methods using perceptual criteria, J. Appl. Crystallogr. 25 (1992) 495–503.
[35] D. Franke, D.I. Svergun, DAMMIF, a program for rapid ab-initio shape determination in small-angle scattering, J. Appl. Crystallogr. 42 (2009) 342–346.
[36] D.I. Svergun, Restoring low resolution structure of biological macromolecules from solution scattering using simulated annealing, Biophys. J. 76 (1999) 2879–2886.
[37] W. Wriggers, Conventions and workflows for using Situs, Acta Crystallogr. D Biol. Crystallogr. 68 (2012) 344–351.
[38] A. Kihara, Y. Akiyama, K. Ito, A protease complex in the *Escherichia coli* plasma membrane: HflKC (HflA) forms a complex with FtsH (HflB), regulating its proteolytic activity against SecY, EMBO J. 15 (1996) 6122–6131.
[39] C. Yanisch-Perron, J. Vieira, J. Messing, Improved M13 phage cloning vectors and host strains: nucleotide sequences of the M13mp18 and pUC19 vectors, Gene 33 (1985) 103–119.